FINITE STRAINS AND VOLUMETRIC LOCKING STUDIES ON THE MEFG

Rodrigo Rossi
Departamento de Engenharia Mecânica, Universidade de Caxias do Sul, Cidade Universitária, Bloco D, Caxias do Sul, RS, 95070-560, Brazil
rrossi@ucs.br

Marcelo Krajnc Alves
Departamento de Engenharia Mecânica, Universidade Federal de Santa Catarina, Campus Trindade, Florianópolis, SC, 88010-970, Brazil
krajnc@emc.ufsc.br

Abstract. *An analysis of the volumetric locking in the context of the modified element-freee Galerkin method is presented in this paper. The modified element-free Galerkin method, a variation of the traditional element-free Galerkin method, presented in this work enables the direct imposition of the essential boundary conditions due to the kronecker delta property of special shape functions constructed in the neighborhood of the essential boundary. The model assumes the multiplicative decomposition of the deformation gradient into elastic and plastic parts and considers a J_2 elasto-plastic constitutive relationship with a nonlinear isotropic hardening. The constitutive model is written in terms of the rotated Kirchoff stress and the logarithmic strain conjugate measure. A Total Lagrangian formulation is considered. Aspects related to the volumetric locking are numerically investigated and a F-bar methodology type is proposed. Some numerical results are presented in order to attest the performance of the proposed methodology.*

Keywords*: Finite strains, Mesh-free, EFG, Volumetric locking.*

1. Introduction

In this work the EFG method proposed in Alves & Rossi (2003), will be numerically investigated when submitted to large deformation problems. More specifically, the proposed procedure considers: a *Total Lagrangian* description; a multiplicative decomposition of the deformation gradient, into a plastic and an elastic part; and a constitutive formulation, given in terms of the logarithmic deformation measure, ln(**U**), and the rotated *Kirchoff* stress. In this model the elastic response is assumed to be hyperelastic, according to the *Hencky* model, and the plastic model is given in terms of a J_2 model. This hypothesis leads to the incompressibility of the plastic flow and to the so called volumetric locking phenomenon, which occurs if one uses, for instance, a low order finite element approximation when solving plane strains and axisymmetric problems. Such phenomenon is also verified in mesh-free methods.

In this work a type of *F-bar* method is implemented, in the context of the mesh-free methods, and investigated under axisymmetric and plane strain conditions. Such choice is due to the simplicity of implementation of the method, when compared with the other methods, and due to the good results mention in the literature.

2. Modified element-free Galerkin method - brief introduction

The objective of the MEFG method, see Alves and Rossi (2003), is to combine, in a suitable way, two weight functions, in order to explore the smoothness of w^{EFG} and the kronecker delta property of w^{EPF}. The strategy can be shown by considering a body with domain Ω and boundary $\partial\Omega$, where $\partial\Omega = \Gamma_u \cup \Gamma_t$ and $\Gamma_u \cap \Gamma_t = \varnothing$. Here, Γ_u and Γ_t are respectively the part of $\partial\Omega$ with prescribed essential and natural boundary conditions, as illustrated in Figure 1. Notice that the EPuFe weight functions are specified at particles that belong to a neighborhood of Γ_u and the EFG weight functions are specified at the remaining particles of the mesh. This procedure enables the determination of an approximate solution that satisfies accurately the essential boundary condition and is smooth in the entire domain, except for a neighborhood of Γ_u. The MEFG method can be seen as a conventional EFG method, having a set of different weight functions, which is able to automatically select, at each particle, the proper type of weight function and to compute the adequate size of its support.

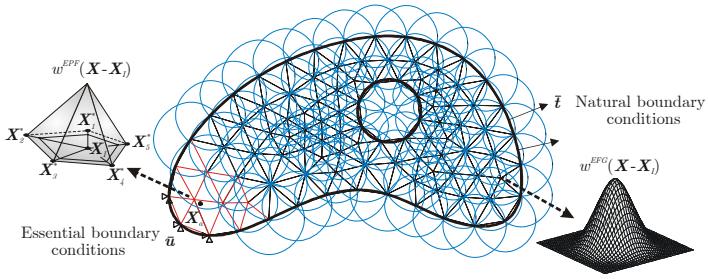

Figure 1 - An example of body coverage by the MEFG

2.1. Mesh-free approximation theory

Using the *Moving Least Square Approximation*, Lancaster and Salkuskas (1981), it is possible to construct an approximation function $u^h(\boldsymbol{X})$ that fits a discrete set of data $\{u_I, I=1\ldots n\}$ such that:

$$u^h(\boldsymbol{X}) = \sum_{I=1}^{n} \Phi_I(\boldsymbol{X}) u_I \,, \tag{1}$$

$$\Phi_I(\boldsymbol{X}) = \boldsymbol{p}(\boldsymbol{X}) \cdot \mathbf{A}(\boldsymbol{X})^{-1} \boldsymbol{b}_I(\boldsymbol{X}), \quad \mathbf{A}(\boldsymbol{X}) = \sum_{I=1}^{n} w(\boldsymbol{X} - \boldsymbol{X}_I)\left[\boldsymbol{p}(\boldsymbol{X}_I) \otimes \boldsymbol{p}(\boldsymbol{X}_I)\right] \quad \text{and} \quad \boldsymbol{b}_I(\boldsymbol{X}) = w(\boldsymbol{X} - \boldsymbol{X}_I)\boldsymbol{p}(\boldsymbol{X}_I) \tag{2}$$

where $\{p_j(\boldsymbol{X}), j=1\ldots m\}$ represents the set of intrinsic base functions and $w(\boldsymbol{X} - \boldsymbol{X}_I)$ is a weight function centered at $\boldsymbol{X}_I$. Here, $\Phi_I(\boldsymbol{X})$ is the global shape function, defined at particle $\boldsymbol{X}_I$, and $\mathbf{A}(\boldsymbol{X})$ is the moment matrix.

The conventional EFG method, Belytschko *et al.* (1994), can de described by the construction of a set of global shape functions, $\Phi_I(\boldsymbol{X})$ defined at particle $\boldsymbol{X}_I$. The particles distribution is not arbitrary since it must satisfy the following condition, Liu *et al.* (1997),

$$card\left\{\boldsymbol{X}_J \,\middle|\, \Phi_J(\boldsymbol{X}) \neq 0\right\} \geq \dim\left[\mathbf{A}(\boldsymbol{X})\right]. \tag{3}$$

In this work, $\boldsymbol{X} \in R^2$ with $\boldsymbol{X}=(X,Y)$, and the intrinsic base functions is $\boldsymbol{p}^T(\boldsymbol{X}) = [1,X,Y]$. Thus, from the condition expressed in Eq.(3), for all $\boldsymbol{X} \in \bar{\Omega}$, there must be at least three particles whose weight functions have a nonzero value at $\boldsymbol{X}$ and whose position vector forms a triangle with a non-zero area. In order to obtain a particle distribution that comply with Eq.(3), we perform a partition of the domain, Ω, into a triangular integration mesh.

Many element-free Galerkin weight functions were proposal in the last years. In this work we use the quartic spline weight function given as:

$$w^{EFG}(r) = \begin{cases} 1 - 6r^2 + 8r^3 - 3r^4, & \text{for} \quad r \leq 1.0 \\ 0, & \text{for} \quad r > 1.0 \end{cases}. \tag{4}$$

Here, $r = r_I / \bar{r}_I$ with $r_I = \left\| \boldsymbol{X} - \boldsymbol{X}_I \right\|$. The radius $\bar{r}_I$, defining the support of $w^{EFG}(\boldsymbol{X} - \boldsymbol{X}_I)$, is determined by

$$\bar{r}_I = s \cdot r_{I\max}, \qquad s > 1, \quad s \in R \quad \text{with} \quad r_{I\max} = \max_i \left\| \boldsymbol{X}_i - \boldsymbol{X}_I \right\|, \quad i \in J_I \tag{5}$$

where J_I represents the set of adjacent particles associated with $\boldsymbol{X}_I$.

Now, in the conventional EFG method, the global shape functions $\{\Phi_I(\boldsymbol{X}), I=1\ldots n\}$, do not satisfy, in general, the *kronecker* delta property, i.e., $\Phi_I(\boldsymbol{X}_J) \neq \delta_{IJ}$. As a consequence, it is not possible to enforce the essential boundary conditions, by directly prescribing nodal values. However, special weight functions may be constructed in order to satisfy the *kronecker* delta property. Among them are the extended partition of unity finite element (EPuFe) weight function. A typical support of an EPuFe global shape function is illustrated in Figure 1. Now, in the case where a linear triangular finite element base function is used as a weight function, it is possible derive:

$$w^{EPF}(\boldsymbol{X}^* - \boldsymbol{X}_I) = \begin{cases} \frac{1}{2A}\left[\left(X_i^* Y_{i+1}^* - X_{i+1}^* Y_i^*\right) + \left(Y_i^* - Y_{i+1}^*\right)X + \left(X_{i+1}^* - X_i^*\right)Y\right], \; \boldsymbol{X} \in \text{supp}\left[\Phi_I(\boldsymbol{X})\right] \\ 0, \quad \text{otherwise} \end{cases} \tag{6}$$

Here, $\boldsymbol{X}_i^*$ and $\boldsymbol{X}_{i+1}^*$ are the elements of the adjacent extended node list set of $\boldsymbol{X}_I$, obtained in a counter clockwise sense of the triangular integration cell whose area is A. The usage of an intrinsic base $\boldsymbol{p}^T(\boldsymbol{X}) = [1,X,Y]$ together with a EPuFe weight function satisfy the requirement in Eq.(3) and, therefore, this extension ensures the regularity of $\mathbf{A}(\boldsymbol{X})$. The extended points are determined as:

$$\boldsymbol{X}_i^* = \boldsymbol{X}_i + \varepsilon(\boldsymbol{X}_i - \boldsymbol{X}_I). \tag{7}$$

Notice that, letting $\varepsilon \to 0$, we derive a global shape function that satisfy, in a limiting sense, at a given particle $\boldsymbol{X}_J$, the kronecker delta property. Unless stated contrary the parameters used in the example section are $s = 1.5$ and $\varepsilon = 10^{-4}$.

2. Finite deformation description

2.1. Kinematics of deformation and conjugate stress measure

The model presented in this paper considers the multiplicative decomposition of the deformation gradient $\mathbf{F}$ into an elastic, $\mathbf{F}^e$, and plastic parts, $\mathbf{F}^p$, such that

$$\mathbf{F} = \mathbf{F}^e \mathbf{F}^p \tag{8}$$

with

$$\mathbf{F} = \nabla_X \varphi(\boldsymbol{X}, t). \tag{9}$$

The consideration of a J_2 plasticity model leads to $\det(\mathbf{F}^p) = 1$ and, since $\det(\mathbf{F}) > 0$, implies that $\det(\mathbf{F}^e) > 0$. Thus, the elastic deformation gradient admits a polar decomposition, i.e.,

$$\mathbf{F}^e = \mathbf{R}^e \mathbf{U}^e \tag{10}$$

where $\mathbf{U}^e = \sqrt{\mathbf{C}^e}$ with $\mathbf{C}^e$ being the elastic right Cauchy-Green tensor given by $\mathbf{C}^e = \left(\mathbf{F}^e\right)^T \mathbf{F}^e$ and $\mathbf{R}^e$ being the elastic rotation tensor. The elastic deformation measure used in this work is the logarithmic or *Hencky* strain tensor given by

$$\mathbf{E}^e = \ln\left(\mathbf{U}^e\right). \tag{11}$$

The stress-strain pairs must be such that rate of work density remains preserved. Thus, the conjugate stress associated with the *Hencky* strain is the *rotated Kirchoff* stress $\bar{\boldsymbol{\tau}}$, given by

$$\bar{\boldsymbol{\tau}} = \left(\mathbf{R}^e\right)^T \boldsymbol{\tau} \mathbf{R}^e. \tag{12}$$

2.1. Constitutive formulation

The constitutive model investigated in this work considers a nonlinear isotropic hardening. In the frame work of the thermodynamic of irreversible process, the free energy potential is assumed to be of the form

$$\rho_o \psi\left(\mathbf{E}^e, \alpha\right) = \tfrac{1}{2}\mathbb{D}\mathbf{E}^e \cdot \mathbf{E}^e + \tfrac{1}{2}H\alpha^2 + \left(\sigma_\infty - \sigma_y\right)\left[\alpha + \tfrac{1}{\delta}e^{-\delta\alpha}\right]. \tag{13}$$

where ρ_o is the mass density, and H, δ, σ_∞ and σ_y are material parameters. $\mathbb{D}$ is the standard fourth order elastic constitutive relation. The state equations are given by

$$\bar{\boldsymbol{\tau}} = \rho_o \frac{\partial \psi}{\partial \mathbf{E}^e} = \mathbb{D}\mathbf{E}^e \tag{14}$$

for the rotated *Kirchoff* stress and

$$k = \rho_o \frac{\partial \psi}{\partial \alpha} = H\alpha + \left(\sigma_\infty - \sigma_y\right)\left(1 - e^{-\delta\alpha}\right) \tag{15}$$

for the isotropic hardening stress. This isotropic hardening relation was used by Simo & Armero (1992), and also by Souza Neto *et al.* (1996) where an investigation of the volumetric locking was performed. Moreover, in this work we assume that

$$\bar{\mathbf{D}}^p = \dot{\lambda}\frac{\partial \mathcal{F}}{\partial \bar{\boldsymbol{\tau}}}, \tag{16}$$

and the hardening variable evolution is

$$\dot{\alpha} = -\dot{\lambda}\frac{\partial \mathcal{F}}{\partial k}. \tag{17}$$

The elasto-plastic model used in this work is associative. In this context the yield function assumes the following form,

$$\mathcal{F}\left(\bar{\boldsymbol{\tau}}, k\right) = \sqrt{3J_2} - \left[k\left(\alpha\right) + \sigma_y\right] \tag{18}$$

Here, $\dot{\lambda}$ is the plastic multiplier and must satisfy the following conditions

$$\mathcal{F} \le 0 \qquad \dot{\lambda} \ge 0 \qquad \dot{\lambda}\mathcal{F} = 0. \tag{19}$$

3. Elasto-plastic initial value problem

The elasto-plastic problem presented in the previous section is dependent on the deformation history. Thus, in order to integrate the evolution equations from time step t_n to t_{n+1}, we must solve an initial value problem. The elasto-plastic initial value problem can be stated as, given the deformation history $\mathbf{F}(t), t \in [t_n, t_{n+1}]$ and

$$\mathbf{F}^p\left(t_n\right) = \mathbf{F}_n^p \quad and \quad \alpha\left(t_n\right) = \alpha_n \tag{20}$$

determine $\mathbf{F}_{n+1}^p$ and α_{n+1} such that the Eq.(14), Eq.(16), Eq.(17) and Eq.(19) are satisfied. The strategy employed in the solution of the nonlinear problem comprises two basic steps that are: an elastic predictor and a plastic corrector.

- **Elastic predictor:** The solution is initially assumed as purely hyperelastic and a trial elastic state is computed by

$$\mathbf{F}_{n+1}^{e^{trial}} = \mathbf{F}_{n+1}\left(\mathbf{F}_n^p\right)^{-1} \quad \mathbf{C}_{n+1}^{e^{trial}} = \left(\mathbf{F}_{n+1}^{e^{trial}}\right)^T \mathbf{F}_{n+1}^{e^{trial}} \quad \mathbf{E}_{n+1}^{e^{trial}} = \frac{1}{2}\ln\left(\mathbf{C}_{n+1}^{e^{trial}}\right) \quad \bar{\boldsymbol{\tau}}_{n+1}^{trial} = \mathbb{D}\mathbf{E}_{n+1}^{e^{trial}} \quad \text{and} \quad k_{n+1}^{trial} = k_n \tag{21}$$

- **Plastic corrector:** The plastic corrector phase considers a *return mapping* algorithm that is obtained by the *backward exponential approximation* proposed in Eterovic & Bathe (1990) and Weber & Anand (1990). This phase consists in:
  - Verify the yield function feasibility: The plastic corrector is done only if $\mathcal{F}\left(\bar{\boldsymbol{\tau}}_{n+1}^{trial}, k_{n+1}^{trial}\right) > 0$.
  - Plastic correction: At this point the evolution laws are discretized. The plastic evolution $\dot{\mathbf{F}}^p = \bar{\mathbf{D}}^p\mathbf{F}^p$ is discretized based on the backward exponential approximation resulting in

$$\mathbf{F}_{n+1}^p = \exp\left(\bar{\mathbf{D}}_{n+1}^p\right)\mathbf{F}_n^p. \tag{22}$$

Moreover, after a straightforward manipulation, Eq.(22) reduces to

$$\mathbf{E}_{n+1}^e = \mathbf{E}_{n+1}^{e^{trial}} - \Delta\lambda\mathbf{N}_{n+1} \tag{23}$$

with

$$\mathbf{N}_{n+1} = \left.\frac{\partial \mathcal{F}}{\partial \overline{\boldsymbol{\tau}}}\right|_{n+1}, \quad \overline{\mathbf{D}}^{p}_{n+1} = \Delta\lambda \mathbf{N}_{n+1} \quad \text{and} \quad \mathbf{R}^{e}_{n+1} = \mathbf{R}^{e^{trial}}_{n+1}. \tag{24}$$

The discretized form of the remaining evolution equations is performed by a standard backward Euler method. Summarizing, the solution of plastic corrector phase is obtained by solving, for $\mathbf{E}^{e}_{n+1}$, α_{n+1} and $\Delta\lambda$,

$$\begin{cases} \mathbf{E}^{e}_{n+1} - \mathbf{E}^{e^{trial}}_{n+1} + \Delta\lambda \mathbf{N}_{n+1} \\ \alpha_{n+1} - \alpha_n - \Delta\lambda \\ \mathcal{F}\left(\overline{\boldsymbol{\tau}}_{n+1}, k\left(\alpha_{n+1}\right)\right) \end{cases} = \begin{bmatrix} 0 \\ 0 \\ 0 \end{bmatrix}. \tag{25}$$

4. Total lagrangean formulation

The problem can be enounced as: Determine $\boldsymbol{u}$ such that

$$\begin{aligned} \operatorname{div}\mathbf{P} - \rho_o \boldsymbol{b} &= \boldsymbol{0} \quad in\ \Omega_o \\ \mathbf{P}\boldsymbol{m} &= \boldsymbol{t} \quad in\ \Gamma_t \\ \boldsymbol{u} &= \overline{\boldsymbol{u}} \quad in\ \Gamma_u \end{aligned} \tag{26}$$

where $\mathbf{P}$ is the first Piola-Kirchoff stress, $\boldsymbol{b}$ is the body force vector, $\boldsymbol{m}$ is the outer normal on $\partial\Omega_o$, $\boldsymbol{t}$ is traction vector and $\overline{\boldsymbol{u}}$ is the prescribed displacement.

The called weak form of the Eq.(26), in the incremental form, can be posed as: Determine $\boldsymbol{u}_{n+1} \in H$ such that

$$\mathcal{G}\left(\boldsymbol{u}_{n+1}, \hat{\boldsymbol{u}}\right) = \int_{\Omega_o} \mathbf{P}\left(\boldsymbol{u}_{n+1}\right) \cdot \nabla_{\boldsymbol{X}} \hat{\boldsymbol{u}}\ d\Omega_o - \int_{\Omega_o} \rho_o \boldsymbol{b} \cdot \hat{\boldsymbol{u}}\ d\Omega_o - \int_{\Gamma_{o_t}} \boldsymbol{t} \cdot \hat{\boldsymbol{u}}\ d\Gamma_{o_t} = 0 \quad \forall\, \hat{\boldsymbol{u}} \in H_o. \tag{27}$$

4.1. Linearization and Newton method

The solution of the nonlinear problem in Eq.(27) is achieved through a standard *Newton-Raphson* iteration method. In this context the linearization of the functional $\mathcal{G}\left(\boldsymbol{u}_{n+1}, \hat{\boldsymbol{u}}\right)$ is required. Assuming $\mathcal{G}$ to be sufficiently regular, we derive

$$\mathcal{G}\left(\boldsymbol{u}^{k}_{n+1} + \Delta\boldsymbol{u}^{k}_{n+1}, \hat{\boldsymbol{u}}\right) = \mathcal{G}\left(\boldsymbol{u}^{k}_{n+1}, \hat{\boldsymbol{u}}\right) + D\mathcal{G}\left(\boldsymbol{u}^{k}_{n+1}, \hat{\boldsymbol{u}}\right)\left[\Delta\boldsymbol{u}^{k}_{n+1}\right] \tag{28}$$

where

$$D\mathcal{G}\left(\boldsymbol{u}^{k}_{n+1}, \hat{\boldsymbol{u}}\right)\left[\Delta\boldsymbol{u}^{k}_{n+1}\right] = \int_{\Omega_o} \mathbb{A}\left(\boldsymbol{u}_{n+1}\right) \cdot \nabla_{\boldsymbol{X}}\left(\Delta\boldsymbol{u}^{k}_{n+1}\right) \cdot \nabla_{\boldsymbol{X}} \hat{\boldsymbol{u}}\ d\Omega_o \tag{29}$$

with

$$\left[\mathbb{A}\right]_{ijkl} = \frac{\partial P_{ij}}{\partial F_{kl}} = \frac{\partial \tau_{ip}}{\partial F_{kl}} F^{-1}_{jp} - \tau_{ip} F^{-1}_{jk} F^{-1}_{lp}. \tag{30}$$

4.1.1. Determination of $\mathbb{A}$

By Eq.(30), the determination of $\mathbb{A}$ requires the derivative of the *Kirchoff* stress tensor with respect to the deformation gradient. As already seem, the *Kirchoff* stress is related to the rotated *Kirchoff* stress by Eq.(12). This means that in the determination of Eq.(30) a derivative of the rotated *Kirchoff* stress with respect to the deformation gradient takes place. But as $\overline{\boldsymbol{\tau}}_{n+1} = \hat{\overline{\boldsymbol{\tau}}}_{n+1}\left(\mathbf{E}^{e^{trial}}_{n+1}, (\bullet)_n\right)$ and by using the chain rule of differentiation, we derive

$$\hat{\mathbb{D}} = \frac{\partial \overline{\boldsymbol{\tau}}_{n+1}}{\partial \mathbf{F}_{n+1}} = \frac{\partial \overline{\boldsymbol{\tau}}_{n+1}}{\partial \mathbf{E}^{e^{trial}}_{n+1}} \frac{\partial \mathbf{E}^{e^{trial}}_{n+1}}{\partial \mathbf{C}^{e^{trial}}_{n+1}} \frac{\partial \mathbf{C}^{e^{trial}}_{n+1}}{\partial \mathbf{F}_{n+1}} = \tilde{\mathbb{D}}\mathbb{G}\mathbb{H} \tag{31}$$

The terms $\mathbb{G}$ and $\mathbb{H}$ in Eq.(31) are related with the geometric part of $\hat{\mathbb{D}}$ and are determined by

$$\left[\mathbb{H}\right]_{ijkl} = \frac{\partial C^{e^{trial}}_{n+1_{ij}}}{\partial F_{n+1_{kl}}} = F^{p^{-1}}_{n_{li}} F^{e^{trial}}_{n+1_{kj}} + F^{e^{trial}}_{n+1_{ki}} F^{p^{-1}}_{n_{lj}} \quad \text{and} \quad \mathbb{G} = \frac{\partial \mathbf{E}^{e^{trial}}_{n+1}}{\partial \mathbf{C}^{e^{trial}}_{n+1}} = \frac{\partial}{\partial \mathbf{C}^{e^{trial}}_{n+1}} \ln\left(\mathbf{U}^{e^{trial}}_{n+1}\right) = \frac{1}{2} \frac{\partial}{\partial \mathbf{C}^{e^{trial}}_{n+1}} \ln\left(\mathbf{C}^{e^{trial}}_{n+1}\right) \tag{32}$$

Notice that in the Eq.(32) a derivative of the type $\partial \ln(\mathbf{X}) / \partial \mathbf{X}$ is required, which consists of a derivative of an isotropic tensor function that was investigated in details in Ortiz *et al.* (2001). Moreover, $\tilde{\mathbb{D}}$ is the only contribution related to the constitutive relation in the consistent tangent modulus $\mathbb{A}$. Its determination depends if the state is elastic, $\mathcal{F} \le 0 \rightarrow \tilde{\mathbb{D}} = \mathbb{D}$, or elasto-plastic $\mathcal{F} > 0 \rightarrow \tilde{\mathbb{D}} = \mathbb{D}^{ep}$. Here, the elasto-plastic modulus is

$$\mathbb{D}^{ep} = \frac{d\bar{\boldsymbol{\tau}}_{n+1}}{d\mathbf{E}_{n+1}^{e^{trial}}} = \left(\mathbb{D}^{-1} + \Delta\lambda \frac{\partial \mathbf{N}_{n+1}}{\partial \bar{\mathbf{T}}_{n+1}} - \frac{1}{\frac{\partial \mathcal{F}}{\partial \alpha_{n+1}}} \mathbf{N}_{n+1} \otimes \mathbf{N}_{n+1} \right)^{-1} . \tag{33}$$

5. An F-Bar implementation

The *F-bar* methodology requires that the $\mathbf{F}$ be decomposed into a volumetric and an isochoric component

$$\mathbf{F} = \mathbf{F}_{iso}\mathbf{F}_{vol} \tag{34}$$

with $\mathbf{F}_{iso} = \left[\det(\mathbf{F})\right]^{\frac{1}{3}} \mathbf{F}$ and $\mathbf{F}_{vol} = \left[\det(\mathbf{F})\right]^{-\frac{1}{3}} \mathbf{I}$. Moreover, in the *F-bar* methodology the $\mathbf{F}_{vol}$ is computed as a constant inside the element. Thus, the *F-bar* is defined as

$$\bar{\mathbf{F}} = \mathbf{F}_{iso}\left(\mathbf{F}_a\right)_{vol} = \left(\frac{\det(\mathbf{F})}{\det(\mathbf{F}_a)} \right)^{\frac{1}{3}} \mathbf{F} . \tag{35}$$

Here we consider the average term $\det(\mathbf{F}_a)$ to be computed as

$$\det(\mathbf{F}_a) = \frac{1}{\Omega_e} \int_{\Omega_e} \det(\mathbf{F}) d\Omega_e . \tag{36}$$

The derivation of the internal force in Eq.(27) and the tangent stiffness in Eq.(30) is achieved by making the following composition $\mathbf{P} = \mathbf{P} \circ \phi(\mathbf{F})$ with $\phi(\mathbf{F}) = \bar{\mathbf{F}}$. Thus,

$$[\bar{\mathbb{A}}]_{ijkl} = \frac{\partial P_{ij}}{\partial \bar{F}_{rs}} \frac{\partial \bar{F}_{rs}}{\partial F_{kl}} . \tag{37}$$

6. Examples

6.1. Necking of a circular bar

Here, we consider the analysis of a hypothetical cylindrical bar with the objective of verifying the necking behavior. The model of the problem is illustrated in Figure 2. The model consists of a bar with a length of 53.334 *mm* and a radius of 6.413 *mm*. Due to the symmetry condition, only a quarter of the model is discretized. The model is submitted to a prescribed displacement of u_z = 7 *mm* in the upper region of the bar. To trigger the necking, a small geometric imperfection is introduced in the model. This imperfection consists of a variation of the radius in the central region of 1%, i.e., the radius of the central region is 6.35 *mm*. Similar examples are presented in the works of Simo & Armero (1992) and Souza Neto *et al.* (2002). Figure 2(a) shows the discretization of the domain into the triangular integration cells. The mesh presented in this Figure will be used also in the simulation using the finite element method, employing classical tri6 finite element, with 1379 nodes. Figures 2(b) and 2(c) show the MEFG particle distribution that contains 364 and 1379 nodes/particles, respectively. The material properties used are: κ = 164206,35 MPa, μ = 80193,80 MPa, H = 129.24 MPa, δ = 16.93, σ_∞ = 715 MPa and σ_y = 450 MPa.

Figure 3 shows the comparison among the deformed configurations of the body outline at 85% and 100% of the total prescribed displacement considering the meshes of Figure 2(a) and 2(c) with and without the *F-bar* methodology. Note that at 85% there are no apparent distinctions between the two methods. However, at 100% of the process a discrepant difference is verified in the necking region. Note also that there is a relevant difference, when the *F-bar* methodology is considered.

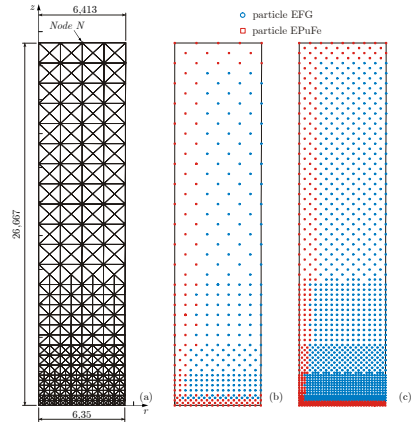

Figure 2 - Integration meshes a) FEM – 1379 nodes, b) MEFG – 364 nodes and c) MEFG – 1379 nodes

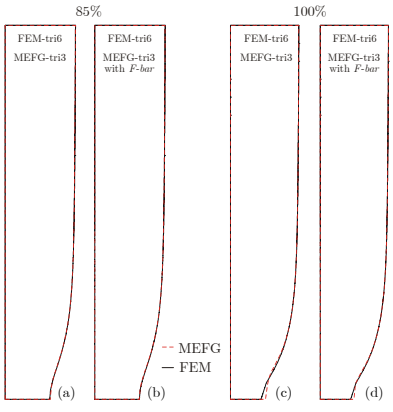

Figure 3 - Comparison among deformed bodies at 85% and 100% of the process.

Figure 4 plots the force *versus* displacement diagram calculated at the top of the structure. It is clear from this figure that the results remain close to one another during a great part of the process. In a certain threshold point, the solution moves away from that achieved by solving a finite element method. Notice again that the implementation of the *F-bar* procedure generates improved results when compared with the finite element solution. In this Figure is also plotted the results presented by Simo & Armero (1992) and Souza Neto *et al.* (1996).

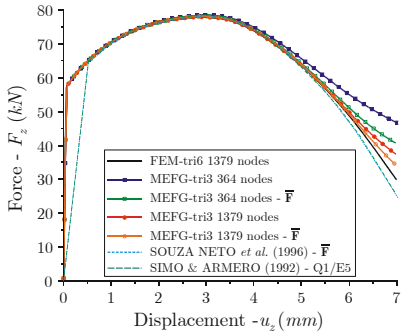

Figure 4 - Comparison between force x displacement at the top of the body

6.1.1 Half simetry

At the last example the necking problem was numerically investigated considering only a quarter of the domain. In this example the central region of the bar suffer high level of deformation. Due to the boundary conditions, symmetry conditions of the problem, the bar central region has great part of this region covered by w^{EPF}. As commented in Alves & Rossi (2003) when only w^{EPF} weight functions are used to form the EFG approximation, its shape functions tends to reproduces a linear interpolation. This means that the deformation gradient is constant approximated. In order to allow the contribution of w^{EFG} in this central region it is proposed that the simulation consider a model based on half symmetry. This model is shown in the Figure 5(a). Figure 5(b) shown the deformed configuration at the end of the process.

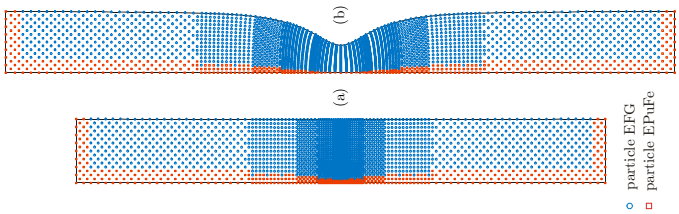

Figure 5 - (a) undeformed model (b) deformed configuration.

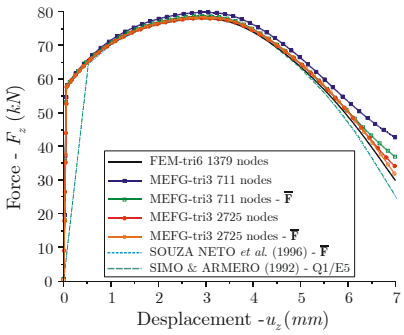

Figure 6 - Force × displacement.

The results in terms of force *versus* displacement are presented in the Figure 6. Again, the force and the displacement are "measured" on the top of the structure. Notice that the MEFG results for this example are more close to those obtained considering FEM-Tri6. Again, it is also plotted the results presented by Simo & Armero (1992) and Souza Neto *et al.* (1996).

6.2. Plane strain localization and mesh dependency

In this example a uniaxial traction model of a rectangular bar under plane strain condition is presented. The dimensions of the bar coincide with those presented in the previous example. This bar is then submitted to a prescribed displacement of $u_z = 5\ mm$ in both the extremities.

In order to prevent the effect of the EPuFe particles, the analysis of the entire body will be considered. The material parameters are the same ones presented in the previous example to less of the associated material parameter with the linear part of the hardening rule that is assumed negative, H = - 12,924 MPa, as suggested by Simo & Armero (1992).

In this example it will be investigated if the solution of the problem suffers from dependence of the integration mesh. Therefore, two integration meshes with the same distribution and number of particles, 861, but with different orientations of the integration cells are proposals. These integration meshes are shown in Figure 7(a), and are called O1, of orientation 1, and 7(b), called of O2. In Figure 7(c) the particle distribution is presented, that in this in case is the same for both meshes. However, this does not mean that the support of the shape functions is precisely the same, as a result of the covering algorithm presented in Alves & Rossi (2003). In this algorithm the determination of support influence parameter s depends

on the maximum distance between the particle and its adjacent particle list, that in fact it is different for each one of the meshes.

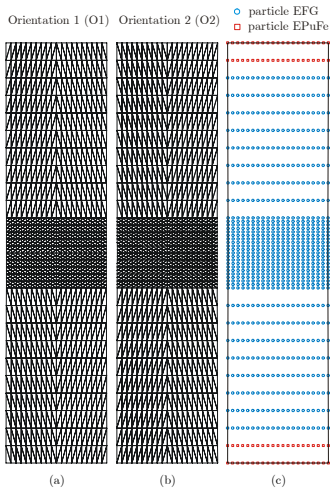

Figure 7 – Integration meshes and particle distribution used in the plane strain example.

For comparison effects, the same analyses will be performed using a triangular finite element tri6. To do that the same integration meshes shown in Figures 7(a) and 7(b) will be used in the analysis. However, in this case the number of degrees of freedom associates the FEM meshes is larger than those used in the analysis by the MEFG. The number of nodes of the FEM-tri6 mesh is 3321.

6.2.1. Finite element results – Tri6

In this section will be presented and discussed only the results obtained for the analysis using the tri6 finite element. Figure 8 shows the deformed meshes achieved at the end of the analysis. Figure 8(a) relates to the mesh with orientation O1 and Figure 8(b) to the mesh with orientation O2. Figures 8(c) and (d) shows a magnification of the region more refined of the deformed Figures 8(a) and (b) respectively. The differences among the two deformed meshes are visible, indicating a strong dependence of the problem solution of the discretization by finite elements.

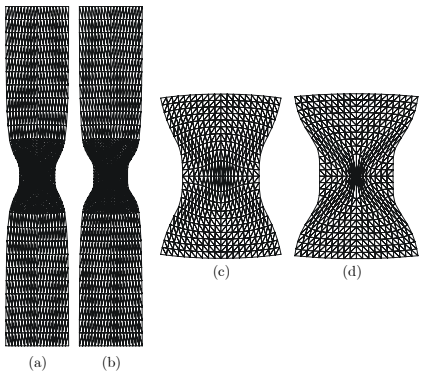

Figure 8 – Deformed configurations. FEM-tri6.

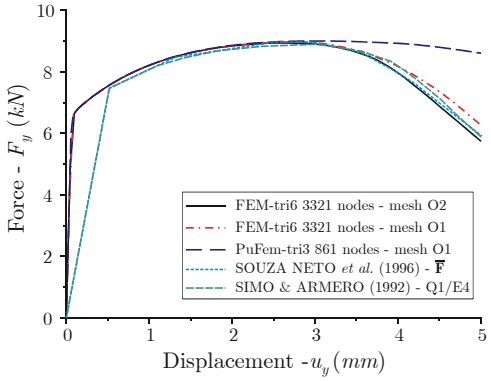

Figure 9 - Force × displacement - FEM-tri6.

Figure 9 shows the force × displacement curve. It can be noticed that the mesh with O2 orientation possesses closer values for prediction of force × displacement when compared with the values presented for those authors.

6.2.2. MEFG results

Figure 10 shows the meshes deformed at the end of the analysis. Figure 10(a) shows the integration mesh with orientation O1 and Figure 10(b) the mesh orientation with O2. Differently of the previous example, there are no observable differences among the deformed configurations. This indicates lower or even no mesh that dependence.

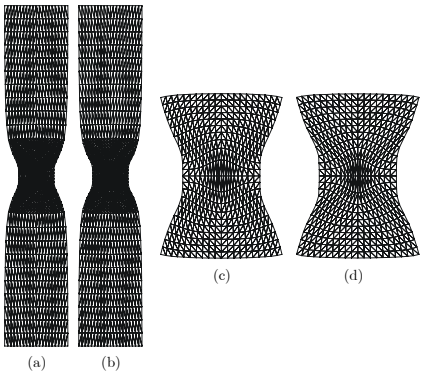

Figure 10 - Deformed configurations. MEFG results.

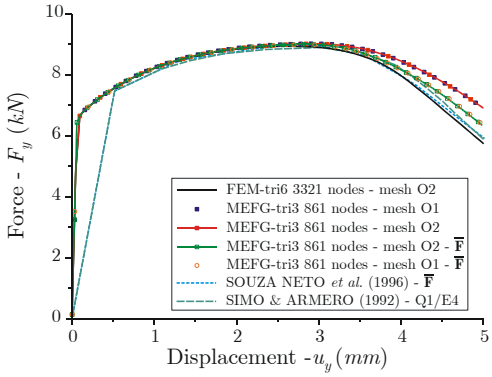

Figure 11 – Force × displacement - MEFG results.

Also, this difference is not evident in the curve force × displacement plotted in the Figure 11. In this graph the results obtained for the analyses without the incorporation of *F-bar* methodology and with *F-bar* methodology are presented considering the integration meshes with orientation O1 and O2 presented in Figure 7(a) and 7(b) respectively.

7. Conclusion

In this work a variation of the traditional element-free *Galerkin* method was numerically investigated under finite strains. Results shown in this paper evidence the presence of volumetric locking in every one elasto-plastic example presented in this paper. Also it shows an improvement of the results since the *F-bar* approach is employed. The results shows that with an improved discretization, a refinement strategy of the domain, mainly in the regions submitted to high plastic flows, it is possible to reduce considerably the locking presence. Moreover, it is also noted that the use of the EPuFe global shape function in the regions submitted to high plastic flows, as in the case of the necking of a circular bar, decrease considerably the effect of *F-bar* methodology. A possible reason for this behavior is the fact that the EPuFe global shape function interpolates **F** as a constant.

8. References

Alves, M.K., Rossi, R. (2003), "A modified element-free Galerkin method with essential boundary conditions, enforced by an extended partition of unity finite element weight function", *International Journal for Numerical Methods in Engineering*, vol. 57, pp. 1523-1552.

Belytschko, T., Lu, Y.Y., Gu, L. (1994), Element-free Galerkin methods, *International Journal for Numerical Methods in Engineering*, vol. 37, pp. 229-256.

Eterovic, A.L., Bathe, K.J. (1990), "A Hyperelastic-Based Large Strain Elasto-Plastic Constitutive Formulation with Combined Isotropic-Kinematic Hardening using the Logarithmic Stress and Strain Measures", *International Journal for Numerical Methods in Engineering*, vol. 30, pp. 1099-1114.

Hughes, T.J.R. (1980), "Generalization of seletive integration procedures to anisotropic and nonlinear media", *International Journal for Numerical Methods in Engineering*, vol. 15, pp. 1413-1418.

Lancaster, P., Salkuskas, K. (1981), "Surfaces generated by moving least square methods", *Mathematical of Computational*, vol. 37, pp. 141-158.

Liu, W.K., Li, S., Belytschko T. (1997), "Moving least-square reproducing kernel methods (I) Methodology and convergence", *Computer Methods in Applied Mechanics and Engineering*, vol. 147, pp. 113-154.

Ortiz M., Radovitzky, R.A., Repeto, E.A. (2001), "The computation of exponential and logarithmic mappings and their fisrt and second linearizations", *International Journal for Numerical Methods in Engineering*, vol. 52, pp. 1431-1441.

Simo, J.C., Armero, F. (1992), "Geometrically Non-Linear Enhanced Strain Mixed Methods and the Method of Incompatible Modes", *International Journal for Numerical Methods in Engineering*, vol. 33, pp. 1413-1449.

Souza Neto E.A., Peric, D., Owen, D.R.J. (2002), Computational Plasticity: Small and Large Strain Finite Element Analysis of Elastic and Inelastic Solids, *Classroom Notes*, University College of Swansea, Wales.

Souza Neto, E.A., Peric, D., Dutko, M., Owen, D.R.J. (1996), "Design of simple low order finite elements for large strain analysis of nearly incompressible solids", *International Journal of Solids and Structures*, vol. 33, pp. 3277-3296.

9. Acknowledgements

The support of the CNPq, Conselho Nacional de Desenvolvimento Científico e Tecnológico, of Brazil is gratefully acknowledged. Grant Numbers: 141806/2000-1 and 304020/2003-6.

10. Responsibility notice

The authors are the only responsible for the printed material included in this paper.